Anisotropic United Atom Model Including the Electrostatic Interactions of Benzene

Patrick Bonnaud, Carlos Nieto-Draghi,* and Philippe Ungerer

Institut Français du Pétrole, 1-4 Avenue de Bois-Préau, 92852 Rueil-Malmaison, Cedex, France

Received: November 20, 2006; In Final Form: January 24, 2007

An optimization including electrostatic interactions has been performed for the parameters of an anisotropic united atoms intermolecular potential for benzene for thermodynamic and transport property prediction using Gibbs ensemble, isothermal–isobaric (NPT) Monte Carlo, and molecular dynamic simulations. The optimization procedure is based on the minimization of a dimensionless error criterion incorporating various thermodynamic data (saturation pressure, vaporization enthalpy, and liquid density) at ambient conditions and at 350 and 450 K. A comprehensive comparison of the new model is given with other intermolecular potentials taken from the literature. Overall thermodynamic, structural, reorientational, and translational dynamic properties of our optimized model are in very good agreement with experimental data. The new model also provides a good representation of the liquid structure, as revealed by three-dimensional spatial density functions and carbon–carbon radial distribution function. Shear viscosity variations with temperature and pressure are very well reproduced, revealing a significant improvement with respect to nonpolar models.

1. Introduction

Benzene is one of the most important organic solvents, and it is used in many industrial applications. Consequently, there is a need of accurate intermolecular potential models that properly describe its equilibrium and transport properties. Several force fields have been proposed in the past decade.[1–18] These models include all atoms (AA), united atoms (UA), anisotropic united atoms (AUA), and exponential six force fields among others. The AUA approach has been successfully applied to different families of hydrocarbons, such as linear[19] and branched alkanes[20] and alkenes,[21] mono- or polyaromatics compounds,[22,23] other sulfur[24,25] compounds.

Previous comparative works show that UA and AUA models of aromatics without electrostatic interaction are capable of reproducing liquid–vapor equilibrium properties quite accurately, keeping the computational cost at minimum.[16] However, the price paid for this simplification is an erroneous description of the liquid structures and intermolecular pair energies with respect to ab initio quantum chemistry calculations.[26] In addition, these simplified potentials present problems when they are used to simulate alkene–aromatic mixtures because their interactions are overestimated.[10,27] Although the electrostatic contribution in benzene represents approximately less than 10% of the total intermolecular energy, this contribution is required to describe correctly the behavior of benzene under different conditions. This relatively low importance of the electrostatic interactions in liquid benzene explains why it is possible to model liquid–vapor equilibrium for pure benzene without explicit inclusion of this interaction.

The situation is completely different in other conditions such as the process of crystallization of benzene,[28,29] the interaction of benzene with polar molecules,[30–34] or the adsorption of benzene into charged alumino-silicate solids.[35–37] In these examples, it is crucial to well describe the presence of the π-cloud of electrons of this molecule. As we will show, a simple nonelectrostatic model, such as the AUA with six interaction sites, has difficulties reproducing transport properties such as viscosity or diffusion under extreme conditions of pressure. This fact is not surprising because the electrostatic interaction tends to increase the friction at high density due to the slight repulsion between molecules at short distances. In general, an increase of the population of planar displaced structures in the liquid,[26] or perpendicular structures (T-shape) structures close to the melting point,[29] is only observed in models that include electrostatic interactions to mimic the quadrupolar moment of benzene.

It seems that the inclusion of this electrostatic energy is required to have a general and transferable model of benzene that can be applied from equilibrium to transport properties. More realistic AA models, such as the optimized potential for liquid simulations (OPLS) of Jorgensen et al.[1,2] or the recent model developed by Cacelli et al.[18] based on ab initio calculations, could be considered as appropriate approaches. However, from a previous work[16] it appears that the OPLS model reproduces well the properties at ambient conditions but fails in representing the liquid–vapor equilibrium properties in a large range of temperatures. In addition, these models require the computation of 12 Lennard-Jones center of force and 12 electrostatic charges; consequently, the computational cost of using these models is large. In the perspective of modeling larger molecules like long-chain alkylbenzenes and polyaromatics in industrial applications, these models would be sometimes unaffordable.

The objective of this work is to develop an optimal and accurate intermolecular potential model of benzene that accounts for electrostatic interactions. Since our final goal is to apply this model to a wide range of applications from property predictions of equilibrium and transport properties to industrial applications such as adsorption, we have paid special attention at keeping the computational costs of our model at a minimum. The process of optimization followed in this work is in agreement with previous works of potential optimization.[16,38]

We have computed several properties to test the capabilities of our model. In particular, we have compared our simulation

* To whom correspondence should be addressed. E-mail: carlos.nieto@ifp.fr.

AUA Model Including the Interactions of Benzene

J. Phys. Chem. B, Vol. 111, No. 14, 2007 **3731**

results for the liquid−vapor density, vapor pressure, and vaporization enthalpy with the available experimental data. We have extended our analysis comparing the structure of the liquid benzene through the computation of radial distribution functions and spatial density functions at ambient and supercooled temperatures. We have also computed several dynamic properties, such as reorientational and self-diffusion coefficient and shear viscosity, at different thermodynamic conditions. Finally, special emphasis has been put on the relationship between the local structural order of the fluid and the consequences of this effect to other computed properties.

The paper is organized as follows. In Section 2, we present the optimization procedure to obtain the intermolecular potential model. Simulation methods and algorithms employed are described in Section 3. Section 4 and 5 are devoted, respectively, to the main results obtained for the different properties and the conclusions of the work.

2. Optimization Method

2.1. Intermolecular Potential Model. The effective dispersion−repulsion interactions between two atoms or UA (i and j) of different molecules are represented by the Lennard-Jones 6−12 equation

$$U_{LJ} = 4\epsilon_{ij}\left[\left(\frac{\sigma_{ij}}{r_{ij}}\right)^{12} - \left(\frac{\sigma_{ij}}{r_{ij}}\right)^{6}\right] \tag{1}$$

where σ_{ij} and ϵ_{ij} are the Lennard-Jones interaction parameters between sites i and j on different molecules, and $r_{ij} \equiv \mathbf{r}_j - \mathbf{r}_i$ is the separation distance between sites i and j. The electrostatic energy is obtained by summing the pairwise Coulombic interactions between the partial charges belonging to the different molecules

$$U_{elec} = \frac{1}{4\pi\epsilon_0} \sum_{i \neq j} \frac{q_i q_j}{r_{ij}^2} \tag{2}$$

where q_i and q_j are the charges of different centers of interaction and ϵ_0 is the dielectric constant of vacuum. Because the benzene molecule is assumed to be rigid, no stretching, bending, or torsional energy is included.

2.2. Force Field Parameters. The following dimensionless error criterion was used:[38]

$$F = \sum_{i=1}^{n} \frac{(X_i^{mod} - X_i^{exp})^2}{s_i^2} \tag{3}$$

where X_i^{exp} is the reference experimental measurement [either $\ln(P^{sat})$, ΔH_{vap}, ρ_l], X_i^{mod} is the associated computed property, and s_i is the estimated statistical uncertainty on X_i^{mod} estimated by standard block-averaging technique.[39] F is considered to be a function of the parameters y_j to be optimized. The minimization of F with respect to all y_j is made by approximating the function by first-order Taylor expansion. For this purpose, the partial derivatives $\partial X_i^{mod}/\partial y_k$ are evaluated by finite differences with the initial set of parameters.

The electrostatic charges were determined to mimic the quadrupolar moment of benzene (i.e., -28.31×10^{-40} C·m^2 from the work of Dennis et al.,[40] -33.3×10^{-40} C·m^2 from the work of Vbrancich et al.[41,42]). We have placed a positive partial charge in the center of the ring and two negative partial charges representing the π-electron clouds are placed perpen-

TABLE 1: Reference Data and Simulation Conditions Used for the Optimization of AUA Potential Parameters of Benzene[a]

T (K)	simulation conditions	property[b]	AUA 9-sites	exp data[c]
350	GCMC	P^{sat} (kPa)	95.8 (4.7)	91.5
		ΔH_{vap} (kJ/mol)	31.52 (1.7)	30.99
		ρ_l (kg/m^3)	819.2 (0.1)	818.7
450	GCMC	P^{sat} (kPa)	1059 (9.3)	969
		ΔH_{vap} (kJ/mol)	24.59 (1.8)	24.16
		ρ_l (kg/m3)	692.9 (−0.1)	693.4

[a] Percentage of deviation with respect to the experimental data in parenthesis. [b] Vapor pressure (P^{sat}), vaporization enthalpies (ΔH_{vap}), and liquid densities (ρ_l). [c] Experimental data.[44]

dicular to the plane of the molecule in the spirit of the united atom transferable potentials for phase equilibria force field (TraPPE) model of Wick et al.[17] For long separation distances, such a charge model is formally equivalent to an OPLS-like charge distribution with 12 charges. Indeed, every charge distribution with more than a 3-fold symmetry axis that does not bear a dipole moment is characterized by a quadrupole moment on the z symmetry axis, which twice the quadrupole moments along the orthogonal x and y axes.[43]

The negative charges were placed at 0.785 Å from the ring plane for the TraPPE model following an electronic structure calculation for benzene with a quadrupole moment of -23.9×10^{-40} C·m^2. In our case, the central charge corresponds to 8.13 and -4.065 e for the two negative out-of-plane charges placed at a distance of 0.4 Å from the center of the ring. According to this charge configuration, our model reproduces a quadrupole moment of -20.8×10^{-40} C·m^2, which is slightly lower than the experimental values. It is important to remark that using the experimental quadrupole moment for our model provides a good performance in transport properties but poor accuracy in reproducing thermodynamic properties in the liquid−vapor region. This fact is not surprising because our model is a caricature of the real molecule and, in addition it is a simplification to represent dispersion−repulsion interactions with simple Lennard-Jones potentials. The final values and distribution of charges provide a good overall performance of model for different properties.

2.3. AUA Parameter Optimization. We have optimized the CH group of benzene starting from the Lennard-Jones parameters (σ and ϵ) and the AUA offset distance δ (i.e., the distance separating the carbon center to the center of force). In the optimization procedure, we have used as initial sets of values in eq 3 the parameters of our previous AUA model of benzene[16] without electrostatic interactions (i.e., $\sigma = 3.2464$ Å, $\epsilon/k = 89.415$ and $\delta = 0.4071$ Å). Six reference data are related to the equilibrium properties of benzene at 450 and 350 K: the vapor pressure, the vaporization enthalpy, and the liquid density as seen in Table 1. These temperatures were selected because they allow an accurate determination of the equilibrium properties with the Gibbs ensemble. We have used the DIPPR[44] database as input experimental data for the optimization procedure. Only few simulations are required to evaluate the six reference data included in the error criterion. The number of independent reference data is chosen to be larger than the number of parameters optimized to ensure convergence and uniqueness of the results.

The three AUA parameters that need to be optimized in the case of benzene for the CH group are the two Lennard-Jones parameters (ϵ and σ) and the offset distance δ_{AUA} (i.e., the distance separating the carbon center from the force center). The potential parameters from this optimization procedure are

TABLE 2: Different Potential Parameters and Centers of Force of Benzene[a]

model	group	σ (Å)	ϵ/k (K)	q (e)	δ (Å)[b]	Q ($\times 10^{-40}$ C·m²)[c]
AUA 9-sites (this work)	CH	3.361	75.6		0.315	−20.8
	(r_{CC} = 1.4 Å)					
	z = 0.0[d]			8.13		
	z = ± 0.4 Å			−4.065		
	I_{xx}[e]	76.55113	I_{yy}[e]	76.55113	I_{zz}[e]	153.1022
AUA 6-sites (ref 16)	CH	3.2464	89.415		0.4071	
	(r_{CC} = 1.4 Å)					
	I_{xx}[e]	76.55113	I_{yy}[e]	76.55113	I_{zz}[e]	153.1022
TraPPE 9-sites (ref 17)	CH	3.740	48.0			−23.9
	(r_{CC} = 1.4 Å)					
	z = 0.0[d]			2.42		
	z = ± 0.785 Å			−1.21		
	I_{xx}[e]	76.55113	I_{yy}[e]	76.55113	I_{zz}[e]	153.1022
TraPPE 6-sites (ref 10)	CH	3.695	50.5			
	(r_{CC} = 1.4 Å)					
ABD (ref 18)	C	3.42	41.734	−0.126		−24.5
	(r_{CC} = 1.4 Å)		(ξ_C = 1.14)[f]			
	H	2.93	2.53	0.126		
	(r_{CH} = 1.08 Å)		(ξ_H = 1.34)[f]			
	I_{xx}[e]	89.21989	I_{yy}[e]	89.21989	I_{zz}[e]	178.4398
OPLS AA (ref 2)	C	3.55	35.225	−0.115		−23.3
	(r_{CC} = 1.4 Å)					
	H	2.42	15.097	0.115		
	(r_{CH} = 1.08 Å)					
	I_{xx}[e]	89.21989	I_{yy}[e]	89.21989	I_{zz}[e]	178.4398

[a] All models respect the planar hexagonal geometry. [b] Distance from the carbon atom. [c] The experimental value range between −28.3 to −33.3 × 10^{-40} C·m².[41,42] [d] Distance from the center in the axis perpendicular to the plane of the molecule. [e] Principal moments of inertia in (g/mol·Å²). [f] Additional parameter to better describe the width of the potential.
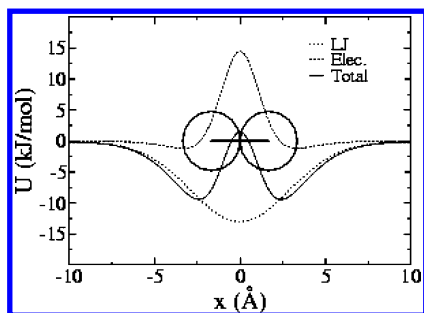

Figure 1. Variation of the potential energy (Lennard-Jones) and electrostatic energy for AUA 9-sites model with the relative position of two benzene molecules approaching with sheet orientation.

given in Table 2. The consequence of including electrostatic interactions is to reduce the ϵ parameter and to slightly increase the σ with respect to our previous AUA model.[16] The δ_{AUA} is reduced, which is normal as it allows to keep the molecular volume approximately constant while σ is increased. Limited changes of Lennard-Jones parameters were also observed for the case of the parametrization of the TraPPE model of benzene with electrostatic interactions.[17]

To better understand the net effect of including electrostatic interactions, we show in Figure 1 the effect of the different intermolecular contributions between two AUA molecules when they approach each other while being located in parallel planes spaced by 4 Å. From this figure, it is clear that the Lennard-Jones energy is attractive while the electrostatic energy is sharply repulsive when the molecules are aligned on the same axis. The net effect of both contributions is a sort of additional "roughness" to the intermolecular interaction of the molecule, as the energy profile shows two minima instead of one in the nonpolar model. An expected consequence is an increased friction between molecules with the new potential, which should result in a significantly different dynamic behavior compared with the previous version of the AUA model.

3. Simulation Methods

3.1. Statistical Ensembles and Monte Carlo Algorithms. Periodic boundary conditions were implemented with the minimum image convention.[39] Dispersion and repulsion interactions were evaluated with a spherical cutoff radius equal to half of the simulation box length for Monte Carlo simulations, associated with standard long-range corrections for the total energy and the pressure. The electrostatic interaction energy was computed by using the Ewald summation with seven vectors in every dimension of the reciprocal space and a scaling parameter α = 2 [π/L] Å^{-1} in the direct space.

3.1.1. Phase Equilibria. The Gibbs ensemble Monte Carlo method[45] was used to compute phase equilibria. The Monte Carlo moves are translations, rigid body rotations, transfers,[4] and volume changes. In transfers, we used a two-step statistical bias involving the selection of a suitable location for the center of mass in a first-step and the test of several orientations in a second-step.[46] The selected probabilities for the various types of moves were generally 0.3 for translations and rotations, 0.395 for transfers, and 0.005 for volume changes. Most simulations were carried out using a total of 220 molecules.

The molar vaporization enthalpy is computed as the difference between the average molar enthalpies of the liquid and of the vapor simulation boxes. The statistical uncertainty on this property is typically 1−2%. The average liquid density was generally determined with a statistical uncertainty of 0.5−1%, but higher values (up to 5%) were found at near-critical temperatures as a result of the larger fluctuations. Once we have computed the vapor−liquid coexistence density curves, the critical temperature was obtained by fitting the critical-scaling law. The molar vaporization enthalpy is computed as the difference between the average molar enthalpies of the liquid and of the vapor simulation boxes. The statistical uncertainty on this property is typically 1−2%. The average liquid density was generally determined with a statistical uncertainty of 0.5− 1%, but higher values (up to 5%) were found at near-critical temperatures as a result of the larger fluctuations. Once we have

AUA Model Including the Interactions of Benzene

J. Phys. Chem. B, Vol. 111, No. 14, 2007 **3733**

computed the vapor−liquid coexistence density curves, the critical temperature was obtained by fitting the critical-scaling law $\rho_l - \rho_v = \lambda(T_c - T)^{0.325}$. The law of rectilinear diameters, $1/2(\rho_l + \rho_v) = \rho_c + \gamma(T - T_c)$, was then used to estimate the critical density.

3.1.2. Liquid Thermodynamic Properties under Ambient Conditions. Simulations in the NPT isothermal−isobaric ensemble were performed on systems of 256 molecules to obtain the saturated liquid properties below 323 K. The molar enthalpy of vaporization is given by the following equation:

$$\Delta H_{vap} = -\langle E_l \rangle + RT \tag{4}$$

where $\langle E_l \rangle$ is the average molar intermolecular potential energy in the simulation. This relationship assumes that (i) the molar volume of the liquid is negligible compared with the vapor and (ii) the vapor is close enough to an ideal gas. These assumptions are correct for benzene below 323 K because the vapor pressure is significantly lower than atmospheric pressure. As liquid properties are not significantly different when the pressure is set to either the experimental or to the model vapor pressure, the NPT simulations at 298 or 293 K have been made at the experimental pressure.

To determine the saturated vapor pressures, the NPT simulations were made at constant intervals in *1/T* scale to use the thermodynamic integration of the Clapeyron equation[47] with second-order numerical integration algorithm.[38] This yields the following working equation

$$\ln(P^{sat}(T_{n+2k})) = \ln(P^{sat}(T_n)) - \frac{2}{R}\Delta(1/T)\sum_{i=1}^{k}\Delta H_{vap}(T_{n+2i-1}) \tag{5}$$

where $\Delta(1/T) = 1/T_i - 1/T_{i+1}$ is the constant spacing of the temperatures on the inverse temperature scale, and T_n is a temperature where a Gibbs ensemble simulation has been performed.

An important aspect in thermodynamic integration is the estimation of the statistical uncertainty. In evaluating the standard deviation on the summation of the right-hand side of eq 5, it appears that the leading term is the uncertainty on $P^{sat}(T_n)$ for the case of the present study. Thus the statistical uncertainty on $P^{sat}(T_{n+2k})$ is at most twice the uncertainty on $P^{sat}(T_n)$.

3.1.3. Liquid Equilibrium Structure. The description of the structure of a molecular fluid in terms of particle densities and distribution functions is an essential tool to understand the behavior of solute−solvent interactions.[48] In particular, three-dimensional (3D) spatial distribution functions (SDF) give information about the local structure of solvents molecules

$$g(\mathbf{r}) = \frac{1}{\rho}\rho(\mathbf{r}) \tag{6}$$

where $g(\mathbf{r})$ is the SDF of a solvent of average number density ρ and $\mathbf{r}$ is a position vector in 3D space. SDF functions can be computed between different interaction sites *a* and *b* for molecular liquids (i.e., $g_{ab}(\mathbf{r})$), and its relation with the well-known site−site radial distribution function (RDF) is evident

$$g_{ab}(r) = \int d\Omega g_{ab}(\mathbf{r}) \tag{7}$$

where $\Omega \equiv (\theta,\phi)$ is the solid angle in the molecular-fixed frame of reference. Previous works employed either solid harmonics or spherical harmonics[49−53] to obtain the distribution function because it permits reducing computational resources and time. However, because computation of transport properties requires

long situations, particularly at high pressures, we have computed SDF directly from spatial volume histograms using the same trajectory used to compute self-diffusion for benzene molecules. A local system of coordinates was placed in the center of each benzene molecule with the *z*-axis pointing in the direction perpendicular to the plane of the molecule (the direction of the quadrupole moment). The *x*-axis was placed on the line joining one of the CH atoms and the center of the molecule, and finally the *y*-coordinate was obtained by the vector product $y = z \times x$. Then polar coordinates were employed to project the separation vector **r** between two molecules into polar coordinates r, θ, and ϕ as shown in Figure 2a. In addition, we have computed the relative angle orientation χ between the normal vectors of benzene molecules as shown in Figure 2b.

A relative orientational SDF can be constructed projecting the function

$$\text{Orientation} = (\cos(\chi) - 0.5) \tag{8}$$

over the isodensity surface probability. This function provides information on the way a fluid is structured. This choice is not unique because other options are available to obtain the same information, especially in locally anisotropic liquids such as water,[53] hydrogen sulfide,[54] acetone and dimethyl-sulfoxide,[55] mixtures of associating fluids,[56,57] or in the study of solids as methane hydrates.[58] Benzene is not as strong a locally ordered fluid as water, but we will use the information provided by the SDF to compare the different models of benzene tested in this work. Moreover, the SDF can help us to visualize the effect that the position and magnitude of the electrostatic charges of the different models may have on the structure of the liquid.

3.2. Dynamic Properties and Algorithms. We have employed a molecular dynamics code developed for rigid or flexible molecules. The equations of motion are integrated through fifth-order predictor corrector Gear-type algorithm.[59] Quaternions were employed to integrate the rotational part of the equations of motions.[60] Because the main objective of this work is to test the predictive capability of the improved potential, all samples were equilibrated at the desired temperature and pressure through NPT rescaling using a weak-coupling bath[61] with long-range corrections[39] for pressure and energy on a 1 ns run. Unless specified otherwise, the production runs are around 10−20 ns for each system (depending on the density and pressure). The integration of the equations of motion was performed with a time step of 2 fs and with a cutoff radius of 10.0 Å. A Verlet nearest-neighbor list was also employed to improve the performance of the simulations. All simulation samples consist of 256 benzene molecules. In all cases, the molecules were initially placed in a cubic box using periodic boundary conditions. Electrostatic interactions were treated using Ewald summation with a cutoff radius of half of the simulation box, in the same way as the thermodynamic calculations. The Nose−Hoover (NVT) thermostat was employed to compute self-diffusion constants, reorientational dynamics, and liquid structure at the desired temperature during 2 ns runs after 1 ns of equilibration using the average density obtained with previous NPT runs.

3.2.1. Reorientational Dynamics. The rotational dynamics of benzene can be analyzed though temperature-dependent reorientational relaxation times, experimentally reported by ^{13}C NMR dipolar spin−lattice relaxation rates and cross-correlation rates between the dipolar relaxation mechanism and the relaxation by chemical-shift anisotropy of the molecule.[62] Deuterated benzene, C_6D_6, is typically used to measure T1 relaxation times of the CH dipole moment vectors in the molecule, which permits

the computation of the correlation times τ and the rotational diffusion constants of benzene. We have computed the reorientational correlation time of two unitary vectors, one parallel ($\hat{\mathbf{e}}_{||}$) and other perpendicular ($\hat{\mathbf{e}}_{\perp}$) to the plane of the benzene molecule (see Figure 1b for details). Two orientational autocorrelation functions can be defined as

$$C_i^l(t) = \langle P_l(\hat{\mathbf{e}}_i(t)\cdot\hat{\mathbf{e}}_i(0))\rangle \qquad (9)$$

where P_l is a Legendre polynomial with $l = 1, 2$ for first- and second-order, respectively. These functions are commonly fitted to the Kohlrausch−Williams−Watts exponential functions[63,64]

$$C_{i,KWW}^l(t) = \exp[(-t/\alpha_i^l)^{\beta_i^l}] \qquad (10)$$

for which the relaxation time can be obtained straightforward as

$$\tau_i^l = \int_0^{\infty} C_{i,KWW}^l(t)\,dt = \frac{\alpha_{lm}}{\beta_{lm}}\Gamma\left(\frac{1}{\beta_{lm}}\right) \qquad (11)$$

Experimentally, one has access to correlation times τ_{lm}, which are normalized over spherical harmonics functions Y_{lm}. Rotational diffusion constants are related to the correlation time for the symmetric benzene diffusor, $\tau_{2m} = 1/(6D^{\perp} + m(D^{||} - D^{\perp}))$. On one hand, we can approximate the perpendicular diffusion constant ($D^{\perp}$) (using $m = 0$ in the spherical harmonic function and assuming that $\tau_{20} \approx \tau_2^{\perp}$,[31] where $\tau_2^{\perp}$ is the relaxation time of the unitary vector $\hat{\mathbf{e}}_{\perp}$) as follows

$$D^{\perp} = \frac{1}{6\tau_2^{\perp}} \qquad (12)$$

On the other hand, for the case of the rotational diffusion constant parallel to the plane of the molecule ($D^{||}$), it depends on two relaxation contributions[62]

$$D^{||} = \frac{3}{16\tau_2^{||} - 4\tau_2^{\perp}} - \frac{1}{12\tau_2^{\perp}} \qquad (13)$$

where $\tau_2^{||}$ is the relaxation time of the unitary vector $\hat{\mathbf{e}}_{||}$. We have also analyzed the approximation of computing the rotational diffusion constant inside (i) the plane of the molecule (D^{2i}) using an expression similar to eq 12 for $\tau_2^{||}$

$$D^{2i} = \frac{1}{6\tau_2^{||}} \qquad (14)$$

To compare our results with previous simulation works, we have computed all relaxation times (τ) fitting our results to eqs 10 and 11. We have also compared our results with relaxation times and rotational diffusion constants obtained with spin−lattice ^{13}C NMR experiments for neat benzene at different temperatures and at ambient pressure.[62]

3.2.2. Self-Diffusion. The self-diffusion coefficient of each molecule has been computed at a constant number of molecules and temperature (NVT) through the mean square displacement, according to the well-known Einstein relation

$$D = \lim_{t\to\infty} \frac{1}{6t}\langle|\mathbf{r}(t) - \mathbf{r}(0)|^2\rangle \qquad (15)$$

[59] where $\mathbf{r}(t)$ is the center of mass vector position of each molecule at time t, $\mathbf{r}(0)$ is the position at $t = 0$, and D is he self-diffusion coefficient.
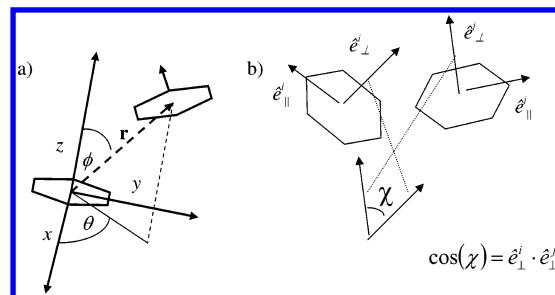

Figure 2. Local system of reference (a) and relative angle orientation χ of normal vectors (b) between benzene molecules. $\hat{\mathbf{e}}_{||}^i$ and $\hat{\mathbf{e}}_{\perp}^i$ are unitary vectors perpendicular and parallel to the plane of the benzene for molecules $i = 1,2$.

3.2.3. Shear Viscosity. The shear viscosity can be calculated for a constant number of particles and fixed temperature, imposing either volume or pressure, in NVT or NPT simulations in thermodynamic equilibrium. Einstein relation, which overcomes the effect of statistical noise observed in the theoretically equivalent Green−Kubo formulation, was employed. The Einstein relation employed in this work is described by Smith and van Gunsteren.[65] However, unlike the original work, we use all the elements of the stress tensor to improve convergence and statistics.[66] The viscosity coefficient is then given by the expression

$$\eta = \frac{1}{20}\frac{V}{k_BT}\lim_{t\to\infty}\frac{d}{dt}[\sum_{\alpha}\langle\Delta P_{\alpha\alpha}^T(t)^2\rangle + 2\sum_{\alpha>\beta}\langle\Delta P_{\alpha\beta}(t)^2\rangle] \quad (16)$$

Here, α and β are indices running over the three Cartesian coordinates, V is the volume (or the average volume in NPT simulations), T is the temperature, and $\Delta P_{\alpha\beta}(t)$ denotes the displacement of the elements of the pressure tensor $P_{\alpha\beta}$ according to

$$\Delta P_{\alpha\beta}(t) = \int_0^t \frac{1}{2}(P_{\alpha\beta}(\tau) + P_{\beta\alpha}(\tau))d\tau \qquad (17)$$

and

$$\Delta P_{\alpha\beta}^T(t) = \int_0^t \left(P_{\alpha\alpha}(\tau) - \frac{1}{3}\sum_{\beta} P_{\beta\beta}(\tau)\right)d\tau \qquad (18)$$

The microscopic expression for the elements of the pressure tensor $P_{\alpha\beta}$ appearing in the integrand of eqs 17 and 18 are given by

$$P_{\alpha\beta}(t) = \frac{1}{V}\left(\sum_i \frac{p_{\alpha i}(t)\,p_{\beta i}(t)}{m_i} + \sum_{i<j}\sum f_{\alpha ij}(t)r_{\beta ij}(t)\right) \quad (19)$$

In eq 19, p_i is the α-component of the momentum of particle i, $f_{\alpha ij}$ is the α-component of the force exerted on particle i by particle j, and $r_{\beta ij}$ is the β-component of the particle−particle vector, $r_{ij} \equiv r_j - r_i$. Here V is the actual volume at the moment of computing $P_{\alpha\beta}$. The viscosity is obtained from eq 16 always after some initial time during which the square displacement is not a linear function of the time.

4. Simulation Results

4.1. Thermodynamic Properties. Simulation results of the new AUA potential for the liquid−vapor density, saturation pressure, and enthalpy of vaporization are compared for different models and the available experimental data in Figures 3, 4, and 5. The estimated critical point for the new model corresponds
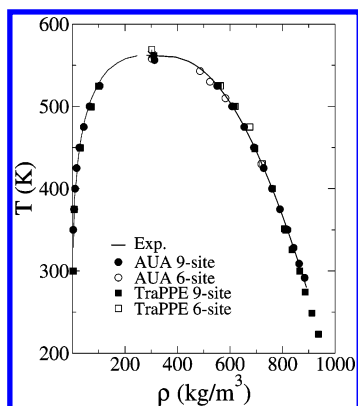
AUA Model Including the Interactions of Benzene

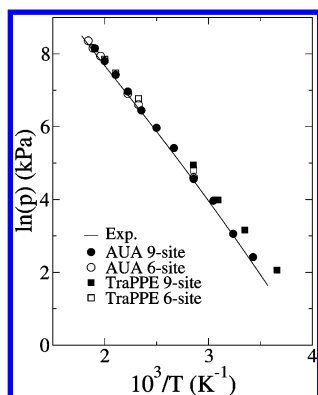*J. Phys. Chem. B, Vol. 111, No. 14, 2007* **3735**

Figure 3. Comparison of the liquid−vapor phase diagram computed for the following models: AUA 9-sites (this work), AUA 6-sites, TraPPE 9-sites, and TraPPE 6-sites with DIPPR correlation based on experimental measurements.[44] The experimental critical point (∗) is also compared with the critical points of each model (same symbols used for the phase diagram). Results for the AUA 6-sites model and TraPPE 6-sites model are taken from ref 16 and ref 10, respectively, and AUA 9-sites model from ref 17.

Figure 4. Comparison of the saturation pressure computed for the following models: AUA 9-sites (this work), AUA 6-sites, TraPPE 9-sites, and TraPPE 6-sites with the DIPPR correlation based on experimental measurements.[44] Results for the AUA 6-sites model and TraPPE 6-sites model are taken from ref 16 and ref 10, respectively, and AUA 9-sites model from ref 17.
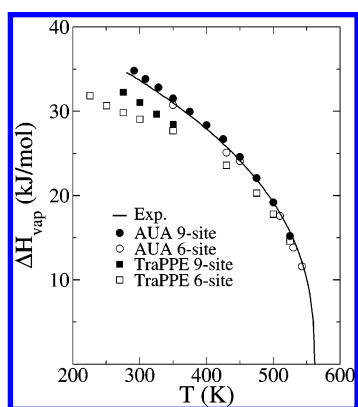

Figure 5. Comparison of the vaporization enthalpy computed for the following models: AUA 9-sites, AUA 6-sites, TraPPE 9-sites, and TraPPE 6-sites with the DIPPR correlation based on experimental measurements.[44] Results for the AUA 6-sites model and TraPPE 6-sites model are taken from ref 16 and ref 10, respectively, and AUA 9-sites model from ref 17.

to a critical temperature $T_c = 556.2$ K, which is 1% lower than the experimental one of 562.2 K, and a critical density $\rho_c = 312.7$ kg/m^3, which is slightly greater than experimental critical density of 304 kg/m^3. The normal boiling temperature, obtained

by interpolation of the vapor pressure, is $T_b = 351$ K (i.e., close to the experimental value of 353.2 K). We can observe the comparison of the liquid−vapor density of the different models with the DIPPR[44] correlation in Figure 3. We have compared our simulation results for the AUA 9-site model with the simulations results obtained with the similar-charged TraPPE 9-sites,[17] the nonpolar AUA 6-sites[16] and the nonpolar TraPPE 6-sites[10] models. From Figure 3, one sees that all models compared represent well the liquid−vapor envelope of benzene. The same conclusion can be made for the critical temperature and density. The situation becomes slightly different when the experimental correlation for the saturation pressure is compared with the same set of models in Figure 4. In this case, the behavior of the AUA models is better (with an AAD of 12.4%), particularly at lower temperatures where the TraPPE 9-sites model slightly overestimates the experimental-saturated pressure. The new AUA 9-sites model presents the best performance in the whole range of temperatures studied. To end the analysis of the thermodynamic properties, we compare the vaporization enthalpy for the four models and the experimental correlation in Figure 5. Both TraPPE models tend to underestimate the vaporization enthalpy at lower temperatures while the AUA models present a good agreement with respect to the quasi-experimental correlation in the whole range of temperatures (with an AAD of 1.7%). To summarize, the newly optimized AUA model from this work provides a prediction of thermo-dynamic properties that is at least equivalent to previous models.

4.2. Liquid Structure. After the analysis of the thermo-dynamic properties, it is possible to conclude that the inclusion of electrostatic interactions is not strictly required. However, previous works have shown that the inclusion of this energy is the only way to reproduce the process of crystallization of benzene.[18,28,29] In fact, Zhao et al. found that when comparing the triple point of the TraPPE 6−sites and 9-sites models, the first one underestimated this property by 130 K ($T_p = 148$ K) whereas the second one predicted a T_p, which is only 10% (253 K) lower than the experimental value of 278.7 K.[44] Recently, Eike et al. computed the melting point of the OPLS model of benzene that accounted for this electrostatic energy employing a reversible solid−liquid transformation path. In this work, they obtained a melting temperature of 255 K, which was close to the experimental one of 278 K. Also, Cacelli et al. computed the melting temperature of their ab initio derived (ABD) model and found it to be 275 K, but predicted a value of 310 K for the OPLS model that was considerably higher than the value reported by the work of Eike.[18]

We have not included in our analysis the determination of the solid−liquid equilibrium, but we are aware of the influence that the electrostatic contribution can have in the local structure of liquid benzene, particularly at low temperatures. For this reason, we have compared the experimental carbon−carbon radial distribution function (ccRDF) of benzene at 298 K and 0.1MPa of Narten et al.[67] with the values obtained with the AUA and TraPPE models in Figure 6a. We can divide our analysis in three zones; the first one at radial distances lower than 5 Å, the second one in the region between 5 and 7 Å, and the last one beyond 7 Å. In the first region at small distances, the AUA 9-sites model is able to reproduce the sharp increase of the RDF at approximately 3 Å and the structure of the shoulder and small peaks experimentally observed between 4 and 5 Å. In the second region, none of the models are able to accurately describe the second shoulder observed in the experimental data. In this case, the AUA 6-sites model and both TraPPE models present a better
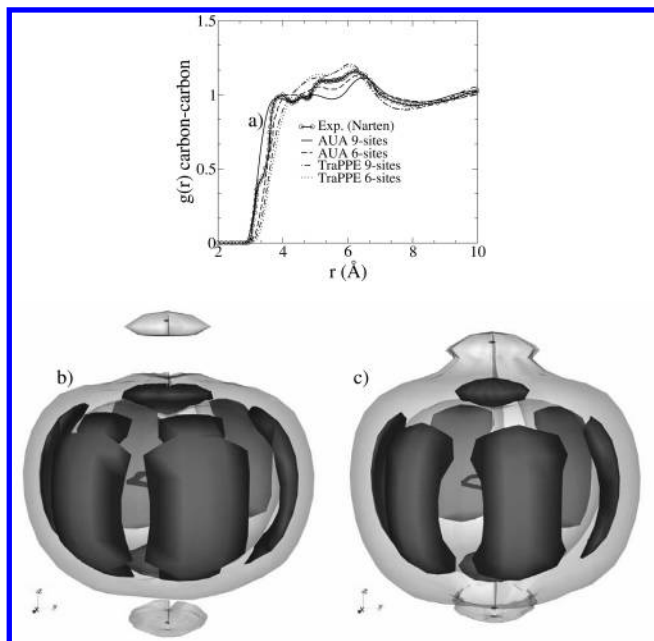
3736 *J. Phys. Chem. B, Vol. 111, No. 14, 2007*

Bonnaud et al.

Figure 6. Carbon−carbon radial distribution function of benzene (a) comparison of the following models: AUA 9-sites, AUA 6-sites, TraPPE 9-sites, TraPPE 6-sites, with the experimental data of Narten[67] at 298K and 0.1 MPa. Carbon−carbon SDFs between benzene molecules at two different isodensity probability surfaces, $g_{cc}(r, \Omega) = 1.7$ (dark region) and $g_{cc}(r, \Omega) = 1.2$ (transparent region) for the AUA 9-sites model (b) and the Trappe 9-sites model (c) at 298K and 0.1 MPa. In figure (a), results for the AUA 6-sites model and TraPPE 6-sites model are taken from ref 16.

description of this region. Finally, almost all models present the same behavior farther away in the third region.

The analysis of the ccRDF is the most common source of comparison of the liquid structure of benzene between experiments and simulations. However, SDFs present the advantage of showing details of the structure of fluids that are embedded in the angular-averaged RDFs. We have computed carbon−carbon SDF of the AUA 9-sites and TraPPE 9-sites models in Figure 6, panels b and c, respectively. In both cases, we represent the 3D isodensity probability for $g_{cc}(r, \Omega) = 1.7$ (dark zones) and $g_{cc}(r, \Omega) = 1.2$ (transparent zones) at 298 K and 0.1 MPa (which corresponds to a density of 873.1 kg/m^3 and 867.9 kg/m^3 for the AUA and TraPPE models, respectively). Integration of the $g_{cc}(r, \Omega)$ function over the solid-angle Ω produces the RDFs presented in Figure 6a. The SDFs can reach values that are locally much greater than RDFs. The explanation is rather simple: RDF include all zones of the space, some of them empty of atoms because they are spatially inaccessible due to excluded volume effects. On average, the internal dark regions correspond to SDF embedded inside a radial distance of 5 Å and the transparent one to SDF inside a radial distance of about 7−8 Å. These zones correspond, respectively, to the first and second region previously discussed in our RDF analysis.

SDFs are accessible indirectly by neutron diffraction experiments,[68,69] using the method of empirical potential structure refinement (EPSR). Unfortunately, to the best of our knowledge there is no experimental SDF available for liquid benzene, and only simulations studies can be reported.[31] However, we can extract useful information analyzing the SDF obtained in our work. In the dark region of Figure 6b, we can observe a strong localization of carbon atoms that are placed in two distinctive regions; perpendicularly placed above and below the central molecule (in radial distances of about 3.5−4 Å) and around the equator of the $g_{cc}(r, \Omega)$. In this last region, we can clearly

appreciate the influence of the excluded volume generated by the 6 Lennard-Jones centers of the model. The volume observed in the dark region of Figure 6c (generated by the TraPPE 9-sites model) presents a similar spatial arrangement than the region observed in Figure 6a; however, the distribution of carbon atoms seems to be more localized in this case. The comparison of the transparent region between the models shows us certain differences, for instance, the AUA 9-sites model is the one that has the most localized carbon atoms at distances lower than 8 Å.

We can tentatively assign the real liquid structure of benzene according to the AUA 9-sites model for distances lower than 5 Å as this model is the one that better reproduces the RDF in this region. A similar case can be considered for the TraPPE 9-sites model in the second region. However, we should keep in mind that many possible SDFs can generate similar RDFs. What can be said is that the real liquid carbon−carbon structure of benzene is definitely closer to AUA 9-site model than TraPPE 9-sites model in the first region.

In Figure 7, we can see the comparison of the SDFs computed in the supercooled liquid region at 260 K and 0.1 MPa with the new model and the TraPPE 9-sites model. Though the crystallization of benzene occurs at 278 K, it is possible in molecular simulations to access the metastable region of supercooled temperatures without problems.[28] In this case, we have compared the spatial distribution of the center of the mass of benzene molecules with respect to the local system of reference defined in Figure 2a at fixed isodensity probability of $g_{cm}(r, \Omega) = 2.0$ between the AUA 9-site model (Figure 7a) and the TraPPE 9-sites model (Figure 7b). In both figures, the structure shown represents a volume embedded is a sphere of approximately 6 Å in radius. In Figure 7a,b, we observe the presence of the same two regions as shown in Figure 6b, although the effect of the temperature reinforces the structure of the liquid around the equator of the central molecule. In contrast, we can say that the structure for the TraPPE 9-sites model presents an arrangement of the isodensity surface that is more homogeneously distributed in the space than the case of the AUA 9-sites model. This means that the AUA 9-sites model strongly localize benzene molecules because the windows of this model are greater than those of the TraPPE model.

To end the structure analysis reproduced by the two models, we have projected the SDFs with the function describing the relative orientation between molecules (eq 8) at the same thermodynamic conditions in Figure 7, panels c (AUA) and d (TraPPE). We can clearly identify the regions in which the molecules are placed in configurations that are mostly perpendicular (orientation = −0.2; for angles greater than 73°) , close to parallel (orientation = 0.2, for angles that are lower than 45°), and an average of all possible configurations (orientation = 0.0). However, according to the spatial distribution in Figure 7c,d we can guess the position of some T-shaped (TS), slipped parallel (SP), and crossed (CR) paradigmatic arrangements of benzene molecules. Only the TraPPE 9-sites model presents some degree of configurations in CR shape; however, we should keep in mind that what we show is the location of average configurations and not the strict configurations as obtained by quantum ab initio computations.[18] In this case, we can clearly see the strong localization of TS molecules in the AUA 9-sites than in the TraPPE 9-sites model.

4.3. Reorientational Dynamics. We have computed the rotational diffusion coefficients and the relaxation times of the AUA 9-sites and the TraPPE 9-sites models describing the reorientation of the vectors parallel to the plane ($\hat{e}_{\parallel}^i$) and perpendicular to the plane ($\hat{e}_{\perp}^i$) of the benzene molecules at 0.1

AUA Model Including the Interactions of Benzene

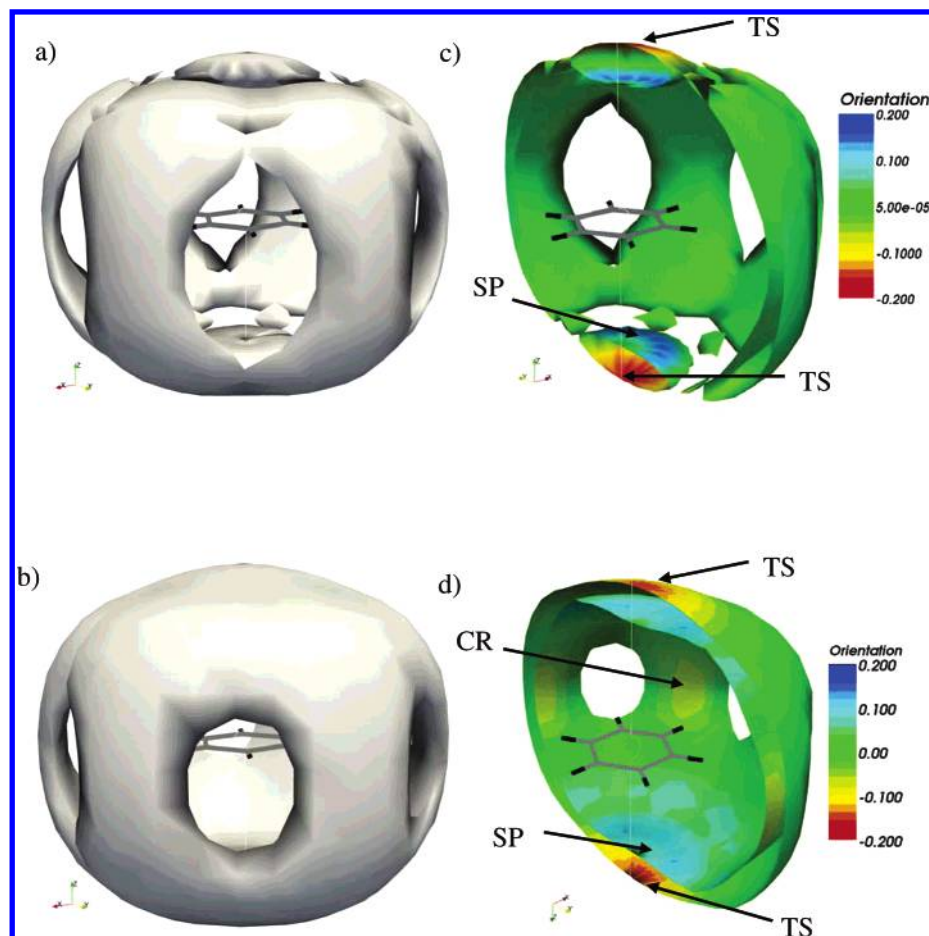*J. Phys. Chem. B, Vol. 111, No. 14, 2007* **3737**

Figure 7. Comparison of the center of mass to center of mass SDFs between benzene molecules at $g_{cm}(r, \Omega) = 2.0$ isodensity probability surface for different models (a) the AUA 9-sites model and (b) TraPPE 9-sites model at 260 K and 0.1 MPa corresponding to a density of 912.9 kg/m^3 and 905.2 kg/m^3 for the AUA and TraPPE models, respectively. Panels (c) and (d) represent the projection of eq 8 over the SDF computed in panels (a) and (b), respectively, (half of the isodensity probability surface is removed for clarity). Benzene molecules inside the figures are placed as guides to understand the SDF and do not represent the geometry of the models. As a guide, we can guess the position of some paradigmatic arrangements of the benzene dimers in panels (c) and (d): TS, CR, and SP.

MPa. Our simulation results are compared with previous simulations obtained with the OPLS model[62] and ABD model[18] and with the available experimental data in Figure 8a−c. Only the charged version of the AUA and TraPPE models are considered for this property because we are mainly interested in the effect that the point charge distribution can have in the reorientational dynamics of the molecule. In general, all models respect the order of magnitude experimentally observed for the rotational relaxation times of benzene molecules. With the exception of the ABD model, the rest of the models respect the relation that $\tau_i^{\perp} > \tau_i^{\parallel}$.[70] Analyzing the reorientation perpendicular to the plane of the molecule, the AUA 9-sites, the ABD, and the OPLS models present values of $\tau_2^{\perp}$ that are closer to the experimental data, while the TraPPE 9-sites model presents values that are systematically too small (a signature of fast rotation). An equivalent behavior for the rotational dynamics was observed between the ABD and OPLS model, as both models present identical geometry, moments of inertia and similar potential energy to describe the dispersion−repulsion interactions. Also, the difference observed between the AUA and TraPPE 9-sites models when having identical moments of inertia (the localization and geometry of the CH groups are the same in both models) present different reorientation dynamics. It seems that inclusion of the AUA displacement δ and the differences in the position and magnitude of the point charges have a combined effect reducing the reorientation of the molecule around the perpendicular plane. Comparing the

relaxation time $\tau_2^{\parallel}$ between the AA OPLS model and the AUA model, we see that they are closer to the experimental data than the TraPPE model. However, in this case the performance of the AUA model is less accurate and the absence of explicit hydrogen atoms reduces the moment of inertia of the molecule with respect to the AA models, affecting the rotation around the main plane of the benzene molecule. Again, the relaxation time $\tau_2^{\parallel}$ obtained with the TraPPE model is too small when compared with the experiments.

The temperature variation of the rotational diffusion constants of the different models and the experimental data at ambient pressure can be seen in Figure 8. For each diffusion coefficient, we have computed the activation energy by an Arrhenius approach and the results of this comparison can be seen in Table 3. In Figure 8a, we compare the rotational diffusion constant obtained by the relation $D^{2i} = 1/(6\tau_2^{\parallel})$ for the different models. On one hand, the coefficients and the activation energy of the AUA model, the OPLS model, and the ABD model are closer to the values experimentally observed. On the other hand, the TraPPE model overestimates the experimental values for D^{2i} and presents an energetic barrier that is approximately half of the experimental one (see Table 3 for details).

The situation is quite different when comparing the temperature variation of the rotational diffusion constant $D^{\parallel}$ at 0.1 MPa obtained with the different models in Figure 8b. We have used eq 13 to compute $D^{\parallel}$ instead of the Einstein relation of the
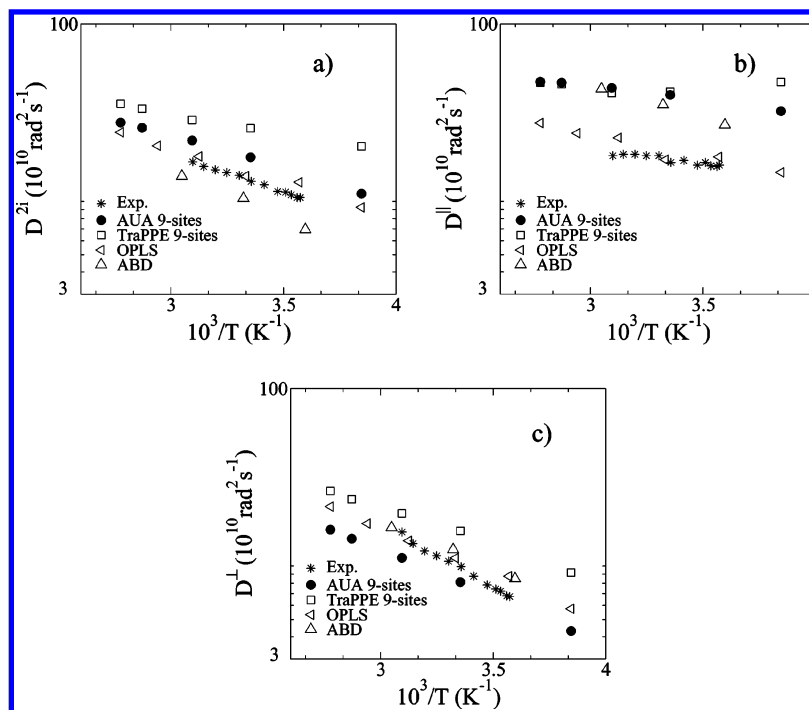
Figure 8. Variation of the rotational diffusion coefficient of benzene with temperature at 0.1 MPa. Comparison of our simulation results using the AUA 9-sites model and TraPPE 9-sites model. Results for OPLS model are taken from the work of Witt et al.[62] and for the rigid version of the ABD model from the work of Cacelli et al.:[18] (a) rotational diffusion coefficient of a vector in the plane of the molecule obtained as $1/(6\tau_2^{||})$, (b) rotational diffusion parallel to the plane of the molecule applying eq 13, and (c) rotational diffusion perpendicular to the plane of the molecule obtained as $1/(6\tau_2^{\perp})$. Experimental data are taken from ref 62.

TABLE 3: Comparison of the Activation Energy Obtained for the Different Dynamic Processes and Models with the Experimental Data at Ambient Pressure[a]

E_a[b]	AUA 9-sites	AUA 6-sites	TraPPE 9-sites	TraPPE 6-sites	ABD	OPLS	exp
D	11.1 (−14)		10.9 (−16)		12.7 (−2.3)	15.1 (16)	13.0[c]
D^{2i}	7.2 (−11)		4.2 (−48)		10.5 (29)	8.2 (1.2)	8.1[d]
$D^{\perp}$	10.2 (−27)		8.1 (−42)		6.6 (−53)	11.5 (−17)	13.9[d]
$D^{||}$	3.0 (3)		0.04 (−99)		9.9 (241)	4.9 (68)	2.9[d]
η	10.7 (2.8)	6.4 (−38)	8.4 (−19)	5.1 (−103)	9.1 (−13)	9.3 (−11)	10.4[e]
AAD (%)[f]	11.6		44.8		67.7	22.6	

[a] Temperature and pressure dependence of the shear viscosity of benzene computed for different models. Results for OPLS model are taken from the work of Witt et al.[62] Results for the rigid version of the ABD model are taken from the work of Cacelli et al.[18] Percentage of deviation with respect to the experimental data in parenthesis. [b] Activation energy in kJ/mol. [c] From ref 71. [d] From ref 62. [e] Computed using the data of ref 72. [f] Absolute average deviation (ADD).

reorientational angle of the molecules used by the work of Witt et al. and Cacelli et al. However, we have verified the validity of this approximation by employing the values of $\tau_2^{\perp}$ and $\tau_2^{||}$ reported in Witt's works to recompute $D^{||}$, and we observe an excellent agreement with the value computed with the Einstein relation. It seems that only the AA models are able to reproduce the values observed in the experimental data. The AUA and TraPPE models reproduce values that are systematically too high. As it was mentioned before, a possible explanation could be the absence of explicit hydrogens and that the three point charges placed in the perpendicular plane are not enough to mimic the rotation around the vertical axis of the molecule. The AA models, presenting point charges in the plane of the molecule, have additional contributions to the torque of the molecule. However, we should remark that the activation energy of the AUA model is in good agreement with the experimental data, while the same quantity obtained with the TraPPE model is too small (see Table 3).

Finally, we compare simulation and experimental values of the rotational diffusion constant $D^{\perp}$ perpendicular to the plane of the molecule in Figure 8c. In agreement with the $\tau_2^{\perp}$ relaxation time discussed before, this coefficient is well

reproduced by the AUA model and the AA models while it is overestimated by the TraPPE model. Surprisingly, the ABD model presents an activation energy that is half of the experiments contrary to the OPLS model, which is the one that better reproduces this property.

4.4. Self-Diffusion Coefficient. The translational self-diffusion coefficients computed with the AUA 9-sites model and the TraPPE 9-sites model at different temperatures at ambient pressure are compared in Figure 9. We have also compared our simulation results with the experimental data of Falcone et al.[71] and previous simulation results for the OPLS and the ABD models. Our results for the AUA model and the TraPPE model agree with the experimental data. As it was stated in the work of Witt et al., the OPLS model presents a diffusion coefficient that is generally too small. The ABD model presents a behavior that is closer to the OPLS model. The activation energies of all models can be compared with the experimental value in Table 3. All models present values that are closer to the experimental data with the ABD model presenting better agreed values. As stated in the works of Witt et al. and Eike et al., it is possible to compute the self-diffusion coefficient at supercooled conditions in molecular simulations without observing any crystal-
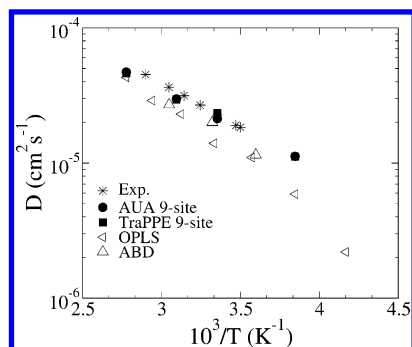
AUA Model Including the Interactions of Benzene

J. Phys. Chem. B, Vol. 111, No. 14, 2007 **3739**

Figure 9. Variation of self-diffusion coefficient of benzene with temperature at 0.1 Mpa computed with the AUA 9-sites model and the TraPPE 9-sites model. Results for OPLS model are taken from the work of Witt et al.[62] and for the rigid version of the ABD model from the work of Cacelli et al.[18] Experimental data are taken from ref 71.
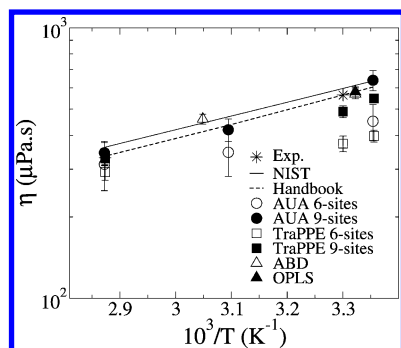

Figure 10. Variation of the shear viscosity of benzene with the temperature at 0.1 MPa computed with the AUA 9-sites model, the AUA 6-sites model, the TraPPE 9-sites model, and the TraPPE 6-sites model. Results for OPLS and for the rigid version of the ABD model are taken from the work of Cacelli et al.[18] The experimental data are taken from ref 72, NIST database, and reference handbook data from ref 73.

lization processes. We have verified this fact in our work by computing this coefficient at 260 K, which is a temperature lower than the experimental melting point of benzene at 278 K without changes in the slope of *D*, as can be seen in Figure 9. The inclusion of certain degree of flexibility in the ABD model seems to improve the performance of the self-diffusion coefficient with respect to its rigid version when the temperature is increased;[18] however, additional degrees of freedom force adopting small time steps with the consequent increment in computational time.

4.5. Viscosity Coefficient. We have analyzed the effect of electrostatic interactions in the computation of the shear viscosity reproduced by the AUA 6-sites and 9-sites and the TraPPE 6-sites and 9-sites at different temperatures at 0.1 MPa in Figure 10 and at a different pressure at 303.15 K in Figure 11. We have compared our simulation results with previous simulations[18] obtained with the OPLS and the ABD models and with the available experimental data[72,73,74] and correlations. In Figure 10, we can observe that the noncharged models underestimate the experimental viscosity at low temperatures (models AUA 6-sites and TraPPE 6-sites have an AAD of 25 and 28%, respectively). Only the models that include electrostatic interactions are able to reproduce correctly this property. On one hand, the OPLS and ABD models slightly overestimate by 4 and 10% the experimental viscosity at 278 and 280 K, respectively. On the other hand, these models behave well at higher temperatures.[18] The AUA 9-sites model presents a total AAD of 7%, which is lower than the 12.5% observed by the TraPPE 9-sites model. Comparing the activation energies of all models in Table
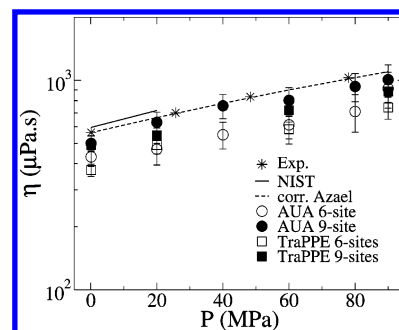

Figure 11. Variation of the shear viscosity of benzene with the pressure at 303.15 K computed with the AUA 9-sites, AUA 6-sites, TraPPE 9-sites, and TraPPE 6-sites models. The experimental data are taken from ref 72, the NIST database, and the Assael correlation.[75]

3, we can observe that the AUA 9-sites model is the one that better reproduces this property. In addition, we observe a general good agreement between the activation energies of the self-diffusion and shear viscosity coefficients at ambient pressure for the charged models.

The knowledge of physical properties of hydrocarbons under fuel injection conditions in the new generation of motors is a good example of an industrial application that can be covered by molecular simulations. In view of this, we have tested the viscosity reproduced by the AUA and TraPPE models under the effect of pressure from 0.1 MPa up to 90 MPa at 303 K. We compare our simulation results with the available experimental data and correlations in Figure 11. The agreement observed between the AUA 9-sites models and the experimental data at different pressures and the correlation of Assael et al.[75] is good; in fact, we obtain a total AAD that is lower than 10%. The behavior of the TraPPE 9-sites model is also acceptable with a total AAD of 13.5%. The viscosities reproduced by the nonelectrostatic models considerably underestimate the experimental data (both the AUA 6-sites model and the TraPPE 6-sites model present a total AAD of about 30%). To understand why charged models behave better than nonelectrostatic ones, the explanation is similar to that used in the process of crystallization of benzene. At high density (or high-packing between molecules), only the combination of the dispersion−repulsion and the electrostatic interactions are able to generate the appropriate orientation between molecules producing enough friction to increase the viscosity of the system. For instance, the electrostatic part in the AUA 9-sites model contributes with an additional "roughness" to the intermolecular interaction of the molecule, as the energy profile shows two minima instead of one in the AUA 6-site model.

5. Conclusions

The main goal of this work is to show the performance of a new AUA intermolecular potential of benzene that accounts for the quadrupolar moment of this molecule. The new potential was adjusted using experimental thermodynamic data at two different temperatures at saturation. During the process of optimization, the viscosity of the model was verified at ambient conditions to ensure coherence with dynamic properties. We have compared our potential with other potentials that include or exclude electrostatic interactions.

Our results in the liquid−vapor region for thermodynamic data show that the new model presents an AAD of 12.3% for the saturation pressure, 1.72% for the vaporization enthalpy, and 0.15% for the liquid density. In addition, we can conclude that the inclusion of electrostatic contribution is not required to well reproduce the experimental equilibrium data and the critical

point. The situation is completely different when solid phases are considered because the process of crystallization requires the promotion of much-ordered T-shape structures. Our analysis of the liquid structure in supercooled conditions, employing spatial density functions projected with mutual orientations, shows the presence of these kind of structures in our model.

The analysis of the reorientational relaxation times shows that the AUA 9-sites model agrees with the experimental data, in particular for the rotational diffusion constant perpendicular to the plane of the molecule (it presents a total AAD of about 18%). Though the TraPPE 9-site model presents a similar arrangement of point charges placed in the perpendicular line to the plane of the molecule and similar quadrupolar moment, our results show that this model overestimates the experimental values of the rotational diffusion perpendicular to the plane (by about 31% of total AAD). However, AUA, TraPPE, and ABD models overestimate the rotational diffusion constant parallel to the plane of the molecule (more than 100%). In general, only the OPLS AA model is able to reproduce both parallel and perpendicular diffusion coefficients with reasonable accuracy (approximately 16%). The experimental self-diffusion coefficient at ambient conditions is reproduced with approximately 10% of AAD for both the AUA and the TraPPE models; however, the AA models compared in our analysis tend to underestimate by a factor of 2 the experimental self-diffusion coefficient.[62]

Finally, we have analyzed the behavior of the different models to reproduce the shear viscosity at different conditions of pressure and temperature. In this case, the AUA 9-sites model presents an AAD of 7%, which is an excellent performance in comparison with the AA approaches (3−6%). The TraPPE 9-sites model presents an AAD of 12.5%, slightly inferior than our new model. The rest of the noncharged models fairly follow the trend observed in experiments for this property (26% for the AUA 6-sites model and 28% for the TraPPE 6-sites model). It is clear from our analysis that this property requires the explicit inclusion of the electrostatic interactions to well reproduce the increment of viscosity when the pressure of the system is increased. The relative orientation between molecules and the correct description of the friction at high densities is only achieved by the models when that includes electrostatic interactions to mimic the quadrupolar moment of benzene molecules.

It is important to state one of the principal achievements of this work: a simple model of benzene can be efficiently parametrized to reproduce several equilibrium, structural, and dynamic properties at the same time. Moreover, the combination of the anisotropic UA approach and the inclusion of electrostatic interaction allows our model to correctly reproduce the temperature dependence of almost all dynamic processes analyzed (in Table 3, an AAD of about 12% for the different activation energies). We have shown that our new model, though having only three point charges, is able to compete accurately with AA models but with 4 times less computational effort. Even with the increase in computer power, computation of properties such as the shear viscosity at extreme conditions remains unaffordable if AA models are employed. In these particular cases, a simplified approach like the one presented in this work is a good alternative.

Supporting Information Available: Tables containing the computed data for thermodynamic and transport properties. This material is available free of charge via the Internet at http://pubs.acs.org.

References and Notes

(1) Jorgensen, W. L.; Madura, J. D. *J. Am. Chem. Soc.* **1984**, *106*, 6638.

(2) Jorgensen, W. L.; Maxwell, D. S.; Tirado-Rives, J. *J. Am. Chem. Soc.* **1996**, *118*, 11225.

(3) Cornell, W. D.; Cieplak, P.; Bayly, C. I.; Gould, I. R.; Merz, K. M.; Ferguson, D. M.; Spellmeyer, D. C.; Fox, T.; Caldwell, J. W.; Kollman, P. A. *J. Am. Chem. Soc.* **1995**, *117*, 5179.

(4) Smit, B.; Karaborni, S.; Siepmann, J. I. *J. Chem. Phys.* **1995**, *102*, 2126.

(5) Sun, H. *J. Phys. Chem. B* **1998**, *102*, 7338.

(6) Martin, M. G.; Siepmann, J. I. *J. Phys. Chem. B* **1998**, *102*, 2569.

(7) Martin, M. G.; Siepmann, J. I. *J. Phys. Chem. B* **1999**, *103*, 4508.

(8) Chen, B.; Siepmann, J. I. *J. Phys. Chem. B* **1999**, *103*, 5370.

(9) Chen, B.; Potoff, J. J.; Siepmann, J. I. *J. Phys. Chem. B* **2001**, *105*, 3093.

(10) Wick, C. D.; Martin, M. G.; Siepmann, J. I. *J. Phys. Chem. B* **2000**, *104*, 8008.

(11) Nath, S. K.; Escobedo, F. A.; de Pablo, J. J. *J. Chem. Phys.* **1998**, *108*, 9905.

(12) Nath, S. K.; Banaszak, B. J.; de Pablo, J. J. *J. Chem. Phys.* **2001**, *114*, 3612.

(13) Nath, S. K.; de Pablo, J. J. *J. Mol. Phys.* **2000**, *98*, 231.

(14) Errington, J. R.; Panagiotopoulos, A. Z. *J. Phys. Chem. B* **1999**, *103*, 6314.

(15) Errington, J. R.; Panagiotopoulos, A. Z. *J. Chem. Phys.* **1999**, *111*, 9731.

(16) Contreras-Camacho, R. O.; Ungerer, P.; Boutin, A.; Mackie, A. D. *J Phys. Chem. B* **2004**, *108*, 14109.

(17) Wick, C. D.; Siepmann, J. I.; Koltz, W. L.; Schure, M. R. *J. Chromatogr., A* **2002**, *954*, 181.

(18) Cacelli, I.; Cinacchi, G.; Prampolini, G.; Tani, A. *J. Am. Chem. Soc.* **2004**, *126*, 14278.

(19) Ungerer, P.; Beauvais, C.; Delhommelle, J.; Boutin, A.; Fuchs, A. H. *J. Chem. Phys.* **2000**, *112*, 5499.

(20) Bourasseau, E.; Ungerer, P.; Boutin, A.; Fuchs, A. H. *Mol. Simul.* **2002**, *28*, 317.

(21) Bourasseau, E.; Haboudou, M.; Boutin, A.; Fuchs, A. H.; Ungerer, P. *J. Chem. Phys.* **2003**, *118*, 3020.

(22) Ahunbay, M. G.; Perez-Pellitero, J.; Contreras-Camacho, R. O.; Teuler, J. M.; Ungerer, P.; Mackie, A. D.; Lachet, V. *J. Phys. Chem. B* **2005**, *109*, 2970.

(23) Contreras-Camacho, R. O.; Ungerer, P.; Ahunbay, M. G.; Lachet, V.; Perez-Pellitero, J.; Mackie, A. D. *J. Phys. Chem. B* **2004**, *108*, 14115.

(24) Delhommelle, J.; Tschirwitz, C.; Ungerer, P.; Granucci, G.; Millie, P.; Pattou, D.; Fuchs, A. H. *J. Phys. Chem. B* **2000**, *104*, 4745.

(25) Perez-Pellitero, J.; Ungerer, P.; Mackie, A. D. *J. Phys. Chem. B* **2006**, submitted.

(26) Smith, G. D.; Jaffe, R. L. *J. Phys. Chem.* **1996**, *100*, 9624.

(27) Wick, C. D.; Martin, M. G.; Siepmann, J. I.; Schure, M. R. *Int. J. Thermophys.* **2001**, *22*, 111.

(28) Eike, D. M.; Maginn, E. *J. Chem. Phys.* **2006**, *124*, 164503.

(29) Zhao, X.; Chen, B.; Karaborni, S.; Siepmann, J. I. *J. Phys. Chem. B* **2005**, *109*, 5368.

(30) Yonezawa, Y.; Nakata, K.; Takada, T.; Nakamura, H. *Chem. Phys. Lett.* **2006**, *428*, 73.

(31) Laaksonen, A.; Stilbs, P.; Wasylishen, R. *J. Chem. Phys.* **1998**, *108*, 455.

(32) Furukata, S.; Ikawa, S. *J. Chem. Phys.* **1998**, *108*, 5159.

(33) Furukata, S.; Ikawa, S. *J. Chem. Phys.* **2000**, *113*, 1942.

(34) Nieto-Draghi, C.; Avalos, J. B.; Contreras, O.; Ungerer, P.; Ridard, J. *J. Chem. Phys.* **2004**, *121*, 10566.

(35) Hahn, J. R.; Jeong, H.; Jeong, S. *J. Chem. Phys.* **2005**, *123*, 244702.

(36) Lachet, V.; Buttefey, S.; Boutin, A.; Fuchs, A. *Phys. Chem. Chem. Phys.* **2001**, *3*, 80.

(37) Su, B. L.; Norberg, V.; Hansenne, C.; Mallmann, A. D. *Adsorption* **2000**, *6*, 61.

(38) Bourasseau, E.; Ungerer, P.; Beauvais, C.; Delhommelle, J.; Boutin, A.; Rousseau, B.; Fuchs, A. *J. Chem. Phys.* **2000**, *112*, 5499.

(39) Allen, M. P.; Tildesley, D. J. *Computer Simulation of Liquids*, 2nd edition; Oxford University Press: Oxford, 1987.

(40) Dennis, G. R.; Ritchie, G. L. D. *J Phys. Chem.* **1991**, *95*, 656.

(41) Vbrancich, J.; Ritchie, G. L. D. *J. Chem. Soc., Faraday Trans. 2* **1980**, *76*, 648.

(42) Vbrancich, J.; Ritchie, G. L. D. *Chem. Phys. Lett.* **1983**, *94*, 63.

(43) Buckingham, A. D. *Adv. Chem. Phys.* **1967**, *12*, 107.

(44) *DIPPR*, version 2005 (Evaluated Standard Thermophysical Property Values); Brigham Young University: Provo, UT, 2005.

(45) Panagiotopoulos, A. Z. *Mol. Phys.* **1987**, *61*, 813.

(46) Bourasseau, E.; Ungerer, P.; Boutin, A. *J. Phys. Chem. B* **2002**, *106*, 5483.

(47) Kofke, D. A. *J. Chem. Phys.* **1993**, *98*, 4149.

(48) Hansen, J. P.; McDonald, I. R. *Theory of Simple Liquids*, 2nd edition; Academic Press: London, 1986.

(49) Yokogawa, D.; Sato, H.; Sakaki, S. *J. Chem. Phys.* **2005**, *123*, 211102.

(50) Nieto-Draghi, C.; Avalos, J. B.; Rousseau, B. *J. Chem. Phys.* **2003**, *118*, 7954.

(51) Sato, H.; Hirataka, F. *Bull. Chem. Soc. Jpn.* **2001**, *74*, 1831.

(52) Svishchev, I. M.; Zassetsky, A. Y. *J. Chem. Phys.* **2000**, *113*, 7432.

(53) Soper, A. K. *J. Chem. Phys.* **1994**, *101*, 6116.

(54) Nieto-Draghi, C.; Mackie, A. D.; Avalos, J. B. *J. Chem. Phys.* **2005**, *123*, 014505.

(55) McLain, S. E.; Soper, A. K. Luzar, A. *J. Chem. Phys.* **2006**, *124*, 074502.

(56) Bowron, D. T.; Moreno, S. D. *J. Phys. Chem. B* **2005**, *109*, 33.

(57) Dougan, L.; Hargreaves, R.; Bates, S. P.; Finney, J. L.; Réat, V.; Soper, A. K. *J. Chem. Phys.* **2005**, *122*, 174514.

(58) Koh, C. A.; Wisbey, R. P.; Wu, X.; Westacott, R. E.; Soper, A. K. *J. Chem. Phys.* **2000**, *113*, 6390.

(59) Frenkel, D.; Smit, B. *Understanding Molecular Simulations: From Algorithms to Applications*, 2nd edition; Academic Press: Amsterdam, 2001.

(60) Evans, D. J. *Mol. Phys.* **1997**, *34*, 317.

(61) Berendsen, H. J. C.; Postma, J. P. M.; van Gunsteren, W. F.; DiNola, A.; Haak, J. R. *J. Chem. Phys.* **1984**, *81*, 3684.

(62) Witt, R.; Sturz, L.; Dölle, A.; Müller-Plathe, F. *J. Phys. Chem. B.* **2000**, *104*, 5716.

(63) Kohlrausch, F. *Ann. Phys.* **1863**, *119*, 337.

(64) Williams, G.; Watts, D. C. *Trans Faraday Soc*. **1970**, *66*, 80.

(65) Smith, P. E.; van Gunsteren, W. F. *Chem. Phys. Lett.* **1993**, *215*, 315.

(66) Mondello, M.; Grest, G. S. *J. Chem. Phys.* **1997**, *106*, 9327.

(67) Narten, A. H.; *J. Chem. Phys.* **1977**, *67*, 2102.

(68) Soper, A. K. *Mol. Phys.* **2001**, *99*, 1503.

(69) Soper, A. K. *Chem. Phys.* **2000**, *258*, 121.

(70) We suspect that the cause of the discrepancy of the ABD model is a simple error in the nomenclature of Table 6 in this work in ref 18.

(71) Falcone, D.; Douglass, D.; McCall, D. *J. Phys. Chem.* **1967**, *71*, 2754.

(72) Parkhust, H. J.; Jonas, J. *J. Chem. Phys.* **1975**, *63*, 2705.

(73) Lide, D. R. *Handbook of Chemistry and Physics*, 73rd edition; CRC Press: London, 1993.

(74) Landolt-Börstein. *Zahlenwerte und Funktionen, Transport Phänomene*; Springer: Berlin, 1969; Vol. II, part 5.

(75) Assael, J. M.; Papadaki, M.; Wakeham, W. A. *Int. J. Thermophys.* **1991**, *12*, 449.